Geometry dependence on inverse spin Hall effect induced by spin pumping in $Ni_{81}Fe_{19}$/Pt films

H. Nakayama,* K. Ando, K. Harii, T. Yoshino, R. Takahashi, Y. Kajiwara, K. Uchida, and Y. Fujikawa
Institute for Materials Research, Tohoku University, Sendai 980-8577, Japan

E. Saitoh
Institute for Materials Research, Tohoku University, Sendai 980-8577, Japan,
Advanced Science Research Center, Japan Atomic Energy Agency, Tokai 319-1195, Japan,
and CREST, Japan Science and Technology Agency, Sanbancho, Tokyo 102-0075, Japan
(Received 19 July 2011; revised manuscript received 30 January 2012; published 12 April 2012)

Geometric effects on the inverse spin Hall effect (ISHE) induced by the spin pumping driven by the ferromagnetic resonance (FMR) have been investigated quantitatively. We measured the FMR spectra and the electromotive force induced by the ISHE with changing the size and the thickness in $Ni_{81}Fe_{19}$/Pt films. The intensity of generated charge currents due to the ISHE changes systematically with changing the film geometry, which is consistent with the prediction of the ISHE. The experimental results show a clear difference between $Ni_{81}Fe_{19}$ and Pt thickness dependence of the ISHE induced by the spin pumping. With a constant Pt thickness, the intensity of the generated charge current is kept proportional to that of the injected spin-current density, which decreases with increased spin relaxation in the $Ni_{81}Fe_{19}$ layer due to interfacial effect, inversely proportional to its film thickness. On the other hand, reflecting the spin diffusion mechanism in the Pt layer, the charge current decreases significantly with the decrease of the Pt thickness, while injected spin-current density is almost kept constant.

DOI: 10.1103/PhysRevB.85.144408 PACS number(s): 72.25.Ba, 72.25.Rb, 75.47.−m, 76.50.+g

I. INTRODUCTION

Generation and detection of spin currents in solid-state systems have attracted much attention in the field of spintronics.[1–12] One method for generating and detecting spin currents is the combination of the spin pumping[13–22] and the inverse spin Hall effect (ISHE).[23–27] The spin pumping enables spin-current generation from magnetization precession motion at a ferromagnetic/paramagnetic interface; a precessing magnetization in the ferromagnetic layer induces a pure spin current in the attached paramagnetic layer. This spin current is converted into a charge current via the ISHE in the paramagnetic layer, which allows the electric detection of a spin current. The combination of the spin pumping and the ISHE allows direct quantitative measurements of spin currents generated by the spin pumping.[28–44]

The amount of the Gilbert damping enhancement due to the spin pumping, which allows us to know the spin-pumping rate, strongly depends on the thickness of the ferromagnetic layer; the additional damping due to the spin pumping is inversely proportional to the thickness of the ferromagnetic layer.[13–15,22] This enhancement of the damping prevents the efficient spin pumping because a large damping constant limits the cone angle of the magnetization precession. The thickness of the paramagnetic layer is also a key parameter in the spin-pumping-induced ISHE measurements. The intensity of charge currents due to the ISHE depends on the thickness because a spin current injected into the paramagnetic layer decays exponentially due to spin relaxation in the paramagnetic layer. Therefore, thickness dependences of the spin-pumping-induced ISHE are essential for quantitative understanding of spin-pumping-induced ISHE measurements. In this paper, we report systematic measurements of a spin current generated by the spin pumping in the different thicknesses of $Ni_{81}Fe_{19}$/Pt films using the ISHE. The experimental results show that the critical difference between the $Ni_{81}Fe_{19}$ layer and the Pt layer thickness dependences of the charge current generated by the ISHE. The generated charge current is proportional to the injected spin current by changing the thickness of the $Ni_{81}Fe_{19}$ layer. By changing the thickness of the Pt layer, in contrast, the charge current increases even when the almost same intensity of spin currents is injected into the Pt layer. These results are quantitatively well reproduced by using a model based on an equivalent circuit and a phenomenological model of the spin pumping.

II. EXPERIMENTAL PROCEDURE

Figure 1(a) shows a schematic illustration of the sample used in the present study. The samples are $Ni_{81}Fe_{19}$/Pt films comprising a paramagnetic Pt layer and a ferromagnetic $Ni_{81}Fe_{19}$ layer. The Pt layer was sputtered on a thermally oxidized Si substrate, and then the $Ni_{81}Fe_{19}$ layer was evaporated in a high vacuum on the Pt layer. Two electrodes are attached on the Pt layer [see Fig. 1(a)]. Here, the surface of the $Ni_{81}Fe_{19}$ layer is a rectangular shape, where the width w and length l of the $Ni_{81}Fe_{19}$ layer are defined as Fig. 1(a).

For the measurement, the $Ni_{81}Fe_{19}$/Pt film is placed near the center of a TE_{011} microwave cavity at which the magnetic-field component $\mathbf{h}_m$ of the mode is maximized, while the electric-field component $\mathbf{e}_m$ is minimized. During the measurement, a microwave mode with a frequency $f = 9.44$ GHz is excited in the cavity, and an external static magnetic field H along the film plane is applied perpendicular to the direction across the electrodes. Because the magnetocrystalline anisotropy in $Ni_{81}Fe_{19}$ is negligibly small, the magnetization in the $Ni_{81}Fe_{19}$ layer is uniformly aligned along the external magnetic-field direction $\mathbf{H}$. When H and f fulfill the ferromagnetic resonance (FMR) condition,[45]

$$\left(\frac{\omega}{\gamma}\right)^2 = H_{\mathrm{FMR}}(H_{\mathrm{FMR}} + 4\pi M_s), \tag{1}$$

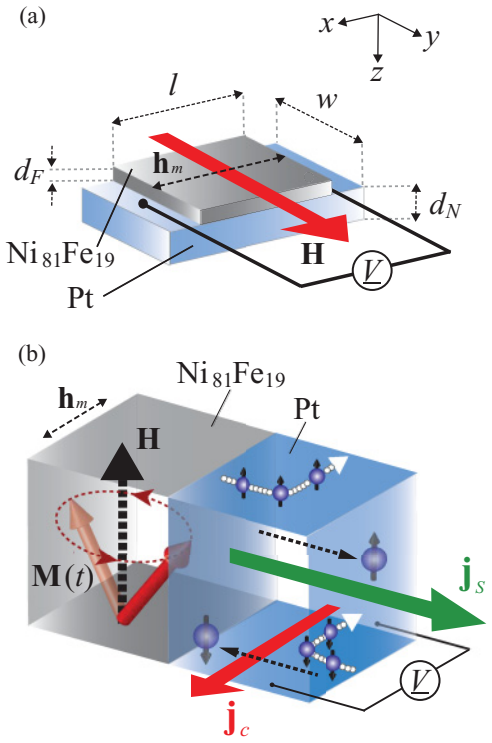

FIG. 1. (Color online) (a) A schematic illustration of the sample system used in the present study. Here, **H**, $\mathbf{h}_m$, d_N, d_F, l, and w denote the external magnetic field, the microwave magnetic field, the thickness of the Pt film and $Ni_{81}Fe_{19}$ film, and the length and the width of the $Ni_{81}Fe_{19}$/Pt bilayer films, respectively. (b) A schematic illustration of the ISHE induced by the spin pumping in the present system. Here, $\mathbf{M}(t)$, $\mathbf{j}_s$, and $\mathbf{j}_c$ denote the magnetization in the ferromagnetic layer, the spatial direction of the spin current generated by the spin pumping, and the charge current induced by the ISHE, respectively. The white arrow in the Pt layer describes electron motion bent by the spin-orbit interaction.

a spin current is injected into the Pt layer by the spin pumping. Here, the dc component of the spin-current density at the interface is theoretically proposed to be[13]

$$j_s^0 = \frac{\omega}{2\pi}\int_0^{\frac{2\pi}{\omega}} \frac{\hbar}{4\pi} g_{\mathrm{eff}}^{\uparrow\downarrow} \frac{1}{M_s^2}\left[\mathbf{M}(t)\times\frac{d\mathbf{M}(t)}{dt}\right]_y dt, \qquad (2)$$

where, ω $(=2\pi f)$, γ, H_{FMR}, $4\pi M_s$, $\hbar$, $g_{\mathrm{eff}}^{\uparrow\downarrow}$, and $\mathbf{M}(t)$ denote the angular frequency of magnetization precession, the gyromagnetic ratio, the resonance magnetic field, the saturation magnetization, the Dirac constant, the real part of the effective spin mixing conductance that includes the contribution of spin accumulation at the interface, and the magnetization, respectively. $[\mathbf{M}(t)\times d\mathbf{M}(t)/dt]_y$ is the y component of $\mathbf{M}(t)\times d\mathbf{M}(t)/dt$. The y axis is defined as Fig. 1(a). This injected spin current $\mathbf{j}_s$ is converted into a charge current $\mathbf{j}_c$ via the ISHE [see Fig. 1(b)] as[23–44]

$$\mathbf{j}_c = \theta_{\mathrm{ISHE}}\left(\frac{2e}{\hbar}\right)\mathbf{j}_s\times\boldsymbol{\sigma}, \qquad (3)$$

giving rise to an electric potential difference between the edges of the Pt layer. Here, θ_{ISHE}, e, and $\boldsymbol{\sigma}$ denote the spin Hall angle, the elementary charge, and the spin-polarization vector of the spin current, respectively. We measured the ISHE induced by the spin pumping with changing the size and the thickness in $Ni_{81}Fe_{19}$/Pt films. All the measurements were performed at room temperature.

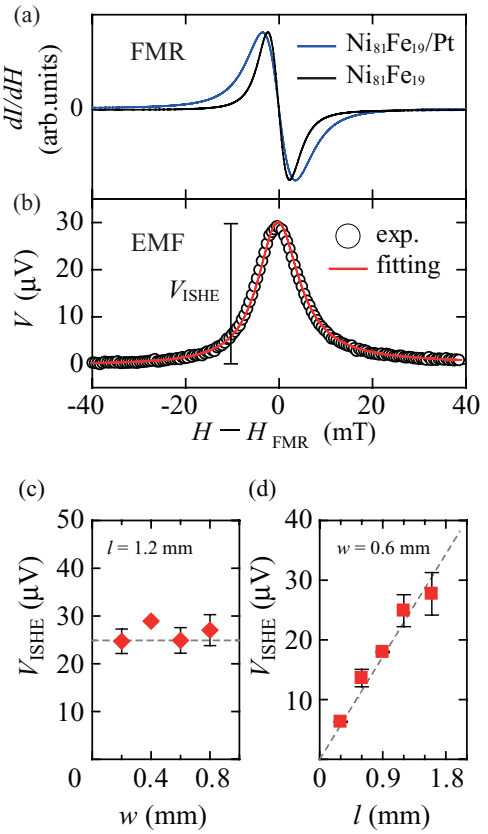

FIG. 2. (Color online) (a) External magnetic field H dependence of the FMR signal measured for the $Ni_{81}Fe_{19}$ ($d_F = 10$ nm)/Pt ($d_N = 10$ nm) bilayer film and single $Ni_{81}Fe_{19}$ ($d_F = 10$ nm) film, where the l and the w are 1.6 and 0.6 mm, respectively. Here, I and H_{FMR} denote the microwave absorption intensity and the resonance magnetic field, respectively. (b) H dependence of the electric voltage V between the electrodes on the Pt films measured for the $Ni_{81}Fe_{19}$/Pt bilayer film under the 200-mW microwave excitation. The shape of V is well reproduced by Eq. (4). The electric voltage induced by the ISHE V_{ISHE} is estimated as the height of the simple Lorentz component in the V spectrum. (c) w dependence of V_{ISHE} under the 200-mW microwave excitation, where l is 1.2 mm. The gray dashed line shows $V_{\mathrm{ISHE}}^{w=0.6\mathrm{mm}}$. (d) l dependence of V_{ISHE} under the 200-mW microwave excitation, where w is 0.6 mm. The gray dashed line shows a linear fit to the data.

III. FILM-SIZE DEPENDENCE OF ISHE INDUCED BY SPIN PUMPING

Figure 2(a) shows the FMR spectra measured for the $Ni_{81}Fe_{19}$ ($d_F = 10$ nm)/Pt ($d_N = 10$ nm) bilayer film and a $Ni_{81}Fe_{19}$ ($d_F = 10$ nm) film with $l = 1.6$ mm and $w = 0.6$ mm [see Fig. 1(a)]. Here, I, d_F, and d_N denote the microwave absorption intensity, the thickness of the $Ni_{81}Fe_{19}$ layer, and the thickness of the Pt layer, respectively. Figure 2(a) shows that the half width at half maximum (HWHM) of $I(H)$, W $(=\omega\alpha/\gamma)$, for the $Ni_{81}Fe_{19}$ film is clearly enhanced

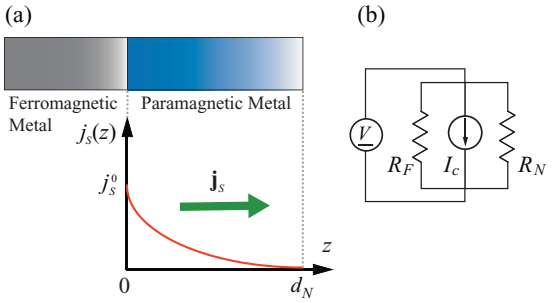

FIG. 3. (Color online) (a) A schematic illustration of the spin-current transport for the z direction in the ferromagnetic/paramagnetic metal bilayer system, which describes the injected spin-current $j_s(z)$ decay along the z direction. Here, j_s^0 denotes the spin-current density at the interface. (b) An equivalent circuit for the ISHE from the spin pumping in the $Ni_{81}Fe_{19}$/Pt bilayer film. The injected spin currents are converted into the charge currents I_c due to the ISHE. Here, R_F and R_N are the resistance of the $Ni_{81}Fe_{19}$ layer and the resistance of the Pt layer, respectively.

by attaching the Pt layer, where α is the Gilbert damping constant. This result demonstrates the emission of a spin current due to the spin pumping; because a spin current carries spin angular momentum, the spin-current emission deprives the magnetization of the spin angular momentum, giving rise to additional magnetization precession damping, or enhances W.

Figure 2(b) shows the electromotive force V for the $Ni_{81}Fe_{19}$ ($d_F = 10$ nm)/Pt ($d_N = 10$ nm) bilayer film under the 200-mW microwave excitation. In the V spectrum, a clear electromotive force peak signal appears around H_{FMR}. The magnitude of the electromotive force due to the ISHE, V_{ISHE}, can be extracted from the V spectrum using the following function:[29]

$$V(H) = V_{ISHE}\frac{\Gamma^2}{(H - H_{FMR})^2 + \Gamma^2} + V_{AHE}\frac{-2\Gamma(H - H_{FMR})}{(H - H_{FMR})^2 + \Gamma^2}, \quad (4)$$

where the first $V_{ISHE}(H)$ and second $V_{AHE}(H)$ terms correspond to the ISHE and anomalous Hall effect (AHE) components, respectively.

In Fig. 2(c), we show the w dependence of V_{ISHE} measured under the 200-mW microwave excitation. V_{ISHE} shows no variation by changing w. In contrast, V_{ISHE} increases linearly with l as shown in Fig. 2(d). These results are consistent with an equivalent circuit model for the $Ni_{81}Fe_{19}$/Pt film shown in Fig. 3(b); in this model, the ISHE voltage is described as $V_{ISHE} = R_N R_F I_c/(R_N + R_F) = d_N\langle j_c\rangle l/(d_N/\rho_N + d_F/\rho_F)$, where R_N, R_F, ρ_N, ρ_F, and $\langle j_c\rangle$ are the resistance of the Pt layer, the resistance of the $Ni_{81}Fe_{19}$ layer, the resistivity of the Pt layer, the resistivity of the $Ni_{81}Fe_{19}$ layer, and the spatial average of the charge current density generated by the ISHE, respectively. Here, we neglected the interface resistance between the $Ni_{81}Fe_{19}$ and Pt layers.

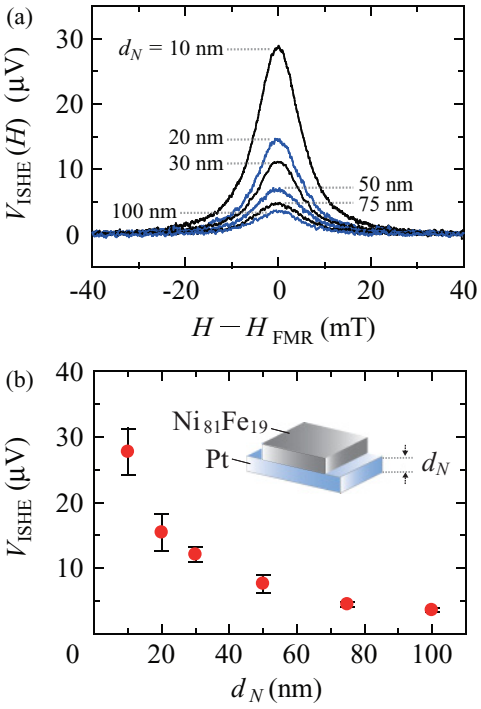

FIG. 4. (Color online) (a) H dependence of V_{ISHE} in different d_N films under the 200-mW microwave excitation, where d_F is 10 nm for all the samples. l and w are 1.6 mm and 0.6 mm, respectively. (b) d_N dependence of V_{ISHE} at the resonance condition under the 200-mW microwave excitation.

IV. FILM-THICKNESS DEPENDENCE OF ISHE INDUCED BY SPIN PUMPING

Figures 4(a) and 4(b) show the Pt layer thickness d_N dependence of V_{ISHE} measured for the $Ni_{81}Fe_{19}$/Pt films under the 200-mW microwave excitation, where d_F is 10 nm for all the samples. l and w are 1.6 and 0.6 mm, respectively. V_{ISHE} shows a monotonic decrease with increasing d_N, which is also explained by the equivalent circuit model as follows. In the $Ni_{81}Fe_{19}$/Pt bilayer film, a spin current j_s^0 injected into the Pt layer decays along the z direction [see Fig. 3(a)] due to spin relaxation as

$$j_s(z) = \frac{\sinh\left(\frac{d_N - z}{\lambda}\right)}{\sinh\left(\frac{d_N}{\lambda}\right)} j_s^0, \quad (5)$$

where $j_s(z)$ and λ denote the spin-current density in the Pt layer and the spin-diffusion length in Pt, respectively. j_s^0 strongly depends on d_N, especially when d_N is smaller than λ. In this film, however, a backflow spin current can be neglected because the Gilbert damping constant α_{eff} for the $Ni_{81}Fe_{19}$/Pt film shows no variation by changing d_N [see the inset to Fig. 5(b)]. By using Eqs. (3) and (5), we obtain the charge current I_c generated by the ISHE in the Pt layer as

$$I_c = \theta_{ISHE} w\left(\frac{2e}{\hbar}\right)\lambda\tanh\left(\frac{d_N}{2\lambda}\right) j_s^0. \quad (6)$$

In Fig. 5(a), we show the d_N dependence of I_c estimated from the V_{ISHE} values shown in Fig. 4(b) using the equivalent circuit model shown in Fig. 3(b): $V_{ISHE} = R_N R_F I_c/(R_N + R_F)$. The experimentally measured I_c values

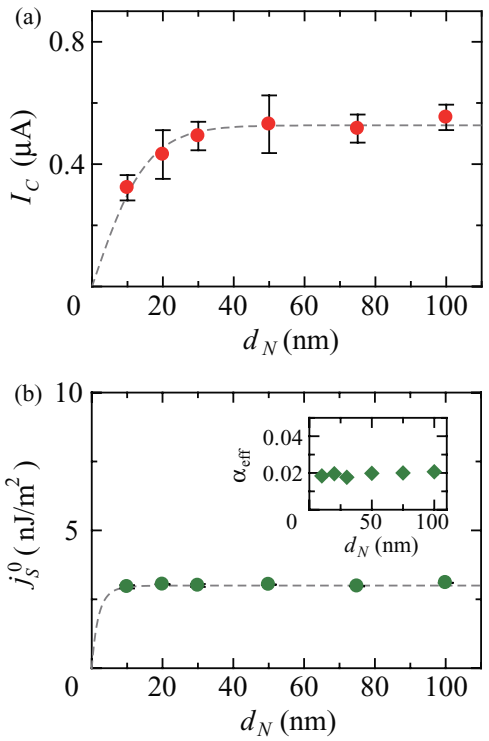

FIG. 5. (Color online) (a) d_N dependence of I_c measured for the $Ni_{81}Fe_{19}$/Pt bilayer films under the 200-mW microwave excitation. The gray dashed curve shows a fitting to Eq. (6), assuming j_s^0 as constant. (b) d_N dependence of j_s^0 estimated from the FMR measurement. The gray dashed curve shows j_s^0 expected from Eqs. (7)–(9). The inset shows d_N dependence of $\alpha_{\rm eff}$ estimated from the FMR spectra measured for the $Ni_{81}Fe_{19}$/Pt bilayer films, where $\alpha_{\rm eff}$ is the Gilbert damping constant for the $Ni_{81}Fe_{19}$/Pt bilayer films.

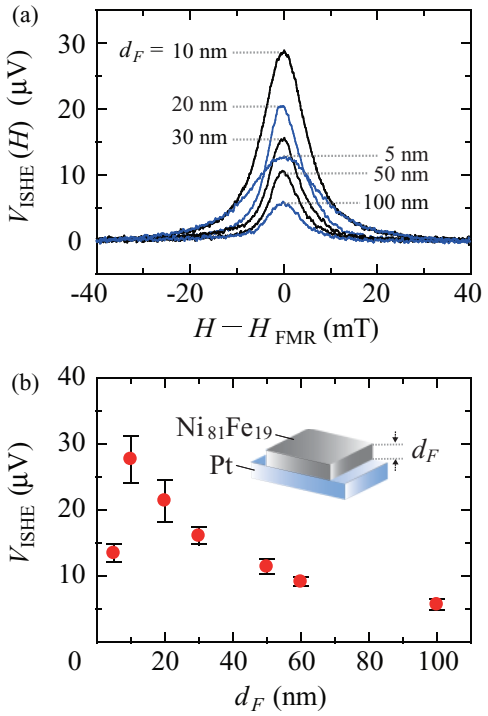

FIG. 6. (Color online) (a) H dependence of $V_{\rm ISHE}$ in different d_F films under the 200-mW microwave excitation, where d_N is 10 nm for all the samples. l and w are 1.6 mm and 0.6 mm, respectively. (b) d_F dependence of $V_{\rm ISHE}$ at the resonance condition under the 200-mW microwave excitation.

are well reproduced using Eq. (6) as shown in Fig. 5(a) with the parameters $\theta_{\rm ISHE}\lambda j_s^0 = 2.9 \times 10^{-19}$ J/m and $\lambda = 7.7 \pm 0.7$ nm, which is comparable to the values obtained by the other methods,[25,46] while some other groups have reported different values (≈3 nm) for the spin-diffusion length in Pt.[11,42] The difference between these values and ours could be explained by the difference in the quality of the thin films.

The spin Hall angle $\theta_{\rm ISHE}$ for the Pt layer can also be obtained from the experimental result shown in Fig. 5(a) with the equivalent circuit model using a phenomenological model of the spin pumping. In this model, the spin-current density j_s^0 generated by the spin pumping is described as[30,33,35]

$$j_s^0 = \frac{g_{\rm eff}^{\uparrow\downarrow}\gamma^2 h_m^2 \hbar[4\pi M_s\gamma + \sqrt{(4\pi M_s)^2\gamma^2 + 4\omega^2}]}{8\pi\alpha_{\rm eff}^2[(4\pi M_s)^2\gamma^2 + 4\omega^2]}. \quad (7)$$

Here, $g_{\rm eff}^{\uparrow\downarrow}$ is related to the Gilbert damping constant $\alpha_{\rm eff}$ for the $Ni_{81}Fe_{19}$/Pt film as[13,31,32]

$$\alpha_{\rm eff} = \alpha_0 + \Delta\alpha = \alpha_0 + \frac{g\mu_B}{4\pi M_s d_F} g_{\rm eff}^{\uparrow\downarrow}, \quad (8)$$

where α_0 and $\Delta\alpha$ denote the intrinsic Gilbert damping constant for the plain $Ni_{81}Fe_{19}$ film, which can be related to W_F, and the additional Gilbert damping constant due to the spin pumping. Here, α_0 is estimated as 1.09×10^{-2} from an FMR spectrum measured for a $Ni_{81}Fe_{19}$ film. g, μ_B, $W_{F/N}$, and W_F are the g factor, the Bohr magneton, the FMR spectral width (HWHM) for the $Ni_{81}Fe_{19}$/Pt film, and the FMR spectral width (HWHM) for the $Ni_{81}Fe_{19}$ film, respectively. The inset to Fig. 5(b) shows the d_N dependence of $\alpha_{\rm eff}$ estimated from $W_{F/N}$. The d_N dependence of j_s^0 estimated from the FMR spectral width using Eqs. (7) and (8) are shown in Fig. 5(b). The gray dashed curve in the same figure shows j_s^0, which is calculated from Eqs. (7) and (8), and the relation[13,47]

$$g_{\rm eff}^{\uparrow\downarrow} = g^{\uparrow\downarrow}\frac{1}{1 + (2\sqrt{\varepsilon/3}\tanh(d_N/\lambda))^{-1}}, \quad (9)$$

with the parameters $4\pi M_s = 0.72$ T, $\gamma = 1.86 \times 10^{11}$ T^{-1}s^{-1}, $g^{\uparrow\downarrow} = 1.13 \times 10^{20}$ m^{-2}, $\varepsilon = 0.1$, and $\lambda = 7.7$ nm. $\varepsilon \approx (Z_{\rm Pt}e^2/\hbar c)^4 = (Z_{\rm Pt}\alpha_{\rm fine})^4$, where $Z_{\rm Pt}$, c, and $\alpha_{\rm fine}$ are the atomic number of Pt, the speed of light, and the fine-structure constant, respectively,[48] which makes $g_{\rm eff}^{\uparrow\downarrow}$ element dependent. Here, $g^{\uparrow\downarrow}$ is the real part of the mixing conductance, which is independent of d_N and the atomic number. When d_N is sufficiently thick, $g^{\uparrow\downarrow}$ defined in Eq. (9) is 3.74 times larger than $g_{\rm eff}^{\uparrow\downarrow}$ in the case of Pt. Therefore, $g^{\uparrow\downarrow}$ obtained here corresponds to $g_{\rm eff}^{\uparrow\downarrow}(d_N \to \infty) = 3.02 \times 10^{19}$ m^{-2}, which agrees reasonably with the previous experimental results.[13,22,30–32,42] $4\pi M_s$, γ, and $g^{\uparrow\downarrow}$ for the $Ni_{81}Fe_{19}$/Pt films were obtained from the FMR spectra. The calculated behavior of j_s^0 is consistent with the experimental results. In contrast to the case of I_c shown in the Fig. 5(a), j_s^0 estimated from the FMR spectra is already saturated around 10 nm, where the value of the saturated j_s^0 is estimated as 3.0 nJ/m^2. Using $\theta_{\rm ISHE}\lambda j_s^0 = 2.9 \times 10^{-19}$ J/m and $\lambda = 7.7$ nm obtained from the best fit of I_c, we obtain

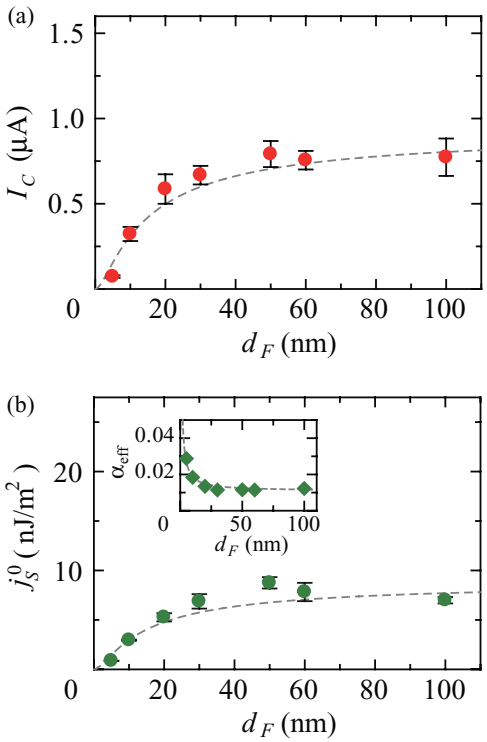

FIG. 7. (Color online) (a) d_F dependence of I_c measured for the $Ni_{81}Fe_{19}$/Pt bilayer films under the 200-mW microwave excitation. The gray dashed curve shows I_c expected from Eqs. (6)–(8). (b) d_F dependence of j_s^0 measured for the $Ni_{81}Fe_{19}$/Pt bilayer films. The gray dashed curve shows j_s^0 expected from Eqs. (7)–(9). The inset shows d_F dependence of α_{eff} estimated from the FMR spectra measured for the $Ni_{81}Fe_{19}$/Pt bilayer films. The gray dashed curve shows α_{eff} expected from Eqs. (8) and (9). The saturation value of α_{eff} agrees well with α_0, which is obtained from an FMR spectrum of the plain $Ni_{81}Fe_{19}$ film, as expected from Eq. (8). Here, α_{eff} is expressed as $\alpha_{eff} = \alpha_0 + \Delta\alpha$.

the spin Hall angle for the Pt layer as $\theta_{ISHE} = 0.013 \pm 0.001$, which is consistent with the previous experimental results,[26,31,32] while some other groups have reported several times larger spin Hall angle than ours.[11,42] This difference could be explained by the difference in the thin-film quality.

We measured also the ISHE induced by the spin pumping with changing d_F. Figures 6(a) and 6(b) show the d_F dependence of V_{ISHE} for the $Ni_{81}Fe_{19}$/Pt bilayer film under the 200-mW microwave excitation, where d_N is 10 nm for all the samples. V_{ISHE} shows monotonic decrease with increasing d_F when d_F is greater than 10 nm. This is due to the reduction of $R_F = \rho_F l/(wd_F)$ with increasing d_F, because $1/V_{ISHE} = 1/(R_F I_c) + 1/(R_N I_c)$. This result also supports that V_{ISHE} is attributed to the ISHE voltage induced by the spin pumping.

In Fig. 7(a), we show the d_F dependence of I_c generated from the ISHE in the Pt films estimated from the ISHE voltage and our equivalent circuit model. The experimental result is well reproduced by Eqs. (6)–(9) with the parameters $4\pi M_s = 0.72$ T, $\gamma = 1.86 \times 10^{11}$ T^{-1}s^{-1}, $g^{\uparrow\downarrow} = 1.13 \times 10^{20}$ m^{-2}, $\varepsilon = 0.1$, $\lambda = 7.7$ nm, and $\theta_{ISHE} = 0.013$ as shown in Fig. 7(a), demonstrating again the validity of the equivalent circuit model. In Fig. 7(b), we show the d_F dependence of j_s^0 estimated from Eqs. (7) and (8). In contrast to the

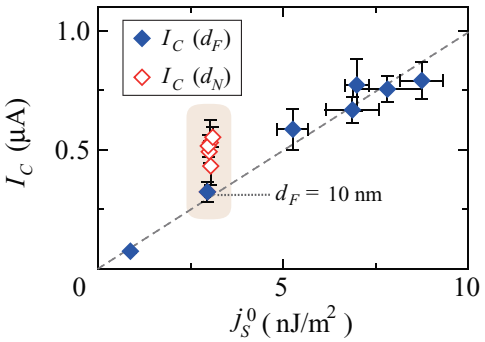

FIG. 8. (Color online) j_s^0 dependence of I_c measured for the $Ni_{81}Fe_{19}$/Pt bilayer films under the 200-mW microwave excitation. The gray dashed line shows linear fit to the experimental data with different d_F, where $d_N = 10$ nm. I_c with different d_F is proportional to j_s^0. In contrast, the values of I_c with different d_N deviate from this proportional relation despite of the constant spin-current density.

d_N dependence of j_s^0 shown in Fig. 5(b), j_s^0 increases with increasing d_F. This is attributed to the decrease of α_{eff} as described in Eqs. (7) and (8). The gray dashed curve in Fig. 7(b) shows the spin-current density at the interface estimated by using the combination of Eqs. (7)–(9) and the above-mentioned parameters. When j_s^0 shows the half of the saturation value, d_F is 16.4 nm for $Ni_{81}Fe_{19}$/Pt junction. This value will be a guideline for designing a high-efficiency spin-current generator and detector using the ISHE induced by the spin pumping and the spin relaxation modulation induced by the spin injection.[9–11] The inset to Fig. 7(b) shows the d_F dependence of α_{eff}. Here, the behavior of α_{eff} is also explained by Eqs. (8) and (9).

Figure 8 shows j_s^0 dependence of I_c, where j_s^0 is estimated from the FMR spectra using Eqs. (7) and (8), and I_c is estimated from the ISHE data using the equivalent circuit model. The gray dashed line shows the linear fit to the experimental data for the $Ni_{81}Fe_{19}$ (d_F)/Pt ($d_N = 10$ nm) films. The experimental results for the $Ni_{81}Fe_{19}$ (d_F)/Pt ($d_N = 10$ nm) films indicate that I_c is proportional to j_s^0. In contrast, for the $Ni_{81}Fe_{19}$ ($d_F = 10$ nm)/Pt (d_N) films, I_c changes even when the same intensity of j_s^0 is injected into the Pt layer. These experimental results show good consistency with Eq. (6). The critical difference between d_N and d_F dependences are attributed to the spin-current decay due to the spin relaxation in the paramagnetic layer as described in Eq. (5).

V. SUMMARY

In summary, we have investigated the geometry dependence on the ISHE induced by the spin pumping in $Ni_{81}Fe_{19}$/Pt bilayer films. The experimental results show clear difference between $Ni_{81}Fe_{19}$ and Pt thickness dependence due to the different mechanism. Reflecting the spin relaxation mechanism in the $Ni_{81}Fe_{19}$ layer due to the interfacial effect, the intensity of the generated charge current with a constant thickness of the Pt layer is kept proportional to that of the injected spin-current density, which decreases with increased spin relaxation in $Ni_{81}Fe_{19}$ layer. On the other hand, reflecting the spin-diffusion mechanism in the Pt layer, the intensity of the generated charge current with a constant thickness of the

$Ni_{81}Fe_{19}$ layer decreases significantly with the decrease of the Pt thickness, while the intensity of the injected spin-current density is almost kept constant. Because the spin pumping and ISHE enable spin-current injection and detection in various systems, these results will provide a guideline for designing a high-efficiency spin-current generator and detector.

ACKNOWLEDGMENTS

This work was supported by a Grant-in-Aid for Scientific Research (A) (Grant No. 21244058) from MEXT, Japan, a Grant-in-Aid for JSPS Fellows from JSPS, Japan, a Grant-in-Aid for Research Activity Start-up (Grant No. 2284005) from MEXT, Japan, Global COE Program "Materials Integration International Center of Education and Research" from MEXT, Japan, a Strategic Information and Communications R&D Promotion Program from MIC (Grant No. 102102001), Japan, the NEXT program from the Cabinet Office, Government of Japan, the Sumitomo Foundation, Japan, Fundamental Research Grant from CREST-JST "Creation of Nanosystems with Novel Functions through Process Integration," and TRF, Japan.

*nakayama@imr.tohoku.ac.jp

[1] I. Zutic, J. Fabian, and S. Das Sarma, Rev. Mod. Phys. **76**, 323 (2004).
[2] S. Maekawa, *Concepts in Spin Electronics* (Oxford University Press, Oxford, 2006).
[3] S. A. Wolf, D. D. Awschalom, R. A. Buhrman, J. M. Daughton, S. von Molnar, M. L. Roukes, A. Y. Chtchelkanova, and D. M. Treger, Science **294**, 1488 (2001).
[4] K. Uchida, S. Takahashi, K. Harii, J. Ieda, W. Koshibae, K. Ando, S. Maekawa, and E. Saitoh, Nature (London) **455**, 778 (2008).
[5] M. Matsuo, J. Ieda, E. Saitoh, and S. Maekawa, Phys. Rev. Lett. **106**, 076601 (2011).
[6] K. Uchida, J. Xiao, H. Adachi, J. Ohe, S. Takahashi, J. Ieda, T. Ota, Y. Kajiwara, H. Umezawa, H. Kawai, G. E. W. Bauer, S. Maekawa, and E. Saitoh, Nat. Mater. **9**, 894 (2010).
[7] Y. K. Kato, R. C. Myers, A. C. Gossard, and D. D. Awschalom, Science **306**, 1910 (2004).
[8] K. Ando, M. Morikawa, T. Trypiniotis, Y. Fujikawa, C. H. W. Barnes, and E. Saitoh, Appl. Phys. Lett. **96**, 082502 (2010).
[9] K. Ando, S. Takahashi, K. Harii, K. Sasage, J. Ieda, S. Maekawa, and E. Saitoh, Phys. Rev. Lett. **101**, 036601 (2008).
[10] K. Ando, H. Nakayama, Y. Kajiwara, D. Kikuchi, K. Sasage, K. Uchida, K. Ikeda, and E. Saitoh, J. Appl. Phys. **105**, 07C913 (2009).
[11] L. Liu, T. Moriyama, D. C. Ralph, and R. A. Buhrman, Phys. Rev. Lett. **106**, 036601 (2011).
[12] S. Takahashi and S. Maekawa, J. Phys. Soc. Jpn. **77**, 031009 (2008).
[13] Y. Tserkovnyak, A. Brataas, G. E. W. Bauer, and B. I. Halperin, Rev. Mod. Phys. **77**, 1375 (2005).
[14] S. Mizukami, Y. Ando, and T. Miyazaki, J. Magn. Magn. Mater. **226–230**, 1640 (2001).
[15] R. Urban, G. Woltersdorf, and B. Heinrich, Phys. Rev. Lett. **87**, 217204 (2001).
[16] B. Heinrich, Y. Tserkovnyak, G. Woltersdorf, A. Brataas, R. Urban, and G. E. W. Bauer, Phys. Rev. Lett. **90**, 187601 (2003).
[17] M. V. Costache, M. Sladkov, S. M. Watts, C. H. van der Wal, and B. J. van Wees, Phys. Rev. Lett. **97**, 216603 (2006).
[18] G. Woltersdorf, O. Mosendz, B. Heinrich, and C. H. Back, Phys. Rev. Lett. **99**, 246603 (2007).
[19] O. Mosendz, G. Woltersdorf, B. Kardasz, B. Heinrich, and C. H. Back, Phys. Rev. B **79**, 224412 (2009).
[20] B. Kardasz and B. Heinrich, Phys. Rev. B **81**, 094409 (2010).
[21] J. Foros, G. Woltersdorf, B. Heinrich, and A. Brataas, J. Appl. Phys. **97**, 10A714 (2005).
[22] A. Ghosh, J. F. Sierra, S. Auffret, U. Ebels, and W. E. Bailey, Appl. Phys. Lett. **98**, 052508 (2011).
[23] S. O. Valenzuela and M. Tinkham, Nature (London) **442**, 176 (2006).
[24] T. Kimura, Y. Otani, T. Sato, S. Takahashi, and S. Maekawa, Phys. Rev. Lett. **98**, 156601 (2007).
[25] L. Vila, T. Kimura, and Y. C. Otani, Phys. Rev. Lett. **99**, 226604 (2007).
[26] M. Morota, Y. Niimi, K. Ohnishi, D. H. Wei, T. Tanaka, H. Kontani, T. Kimura, and Y. Otani, Phys. Rev. B **83**, 174405 (2011).
[27] T. Seki, Y. Hasegawa, S. Mitani, S. Takahashi, H. Imamura, S. Maekawa, J. Nitta, and K. Takanashi, Nat. Mater. **7**, 125 (2008).
[28] C. W. Sandweg, Y. Kajiwara, A. V. Chumak, A. A. Serga, V. I. Vasyuchka, M. B. Jungfleisch, E. Saitoh, and B. Hillebrands, Phys. Rev. Lett. **106**, 216601 (2011).
[29] E. Saitoh, M. Ueda, H. Miyajima, and G. Tatara, Appl. Phys. Lett. **88**, 182509 (2006).
[30] K. Ando, S. Takahashi, J. Ieda, Y. Kajiwara, H. Nakayama, T. Yoshino, K. Harii, Y. Fujikawa, M. Matsuo, S. Maekawa, and E. Saitoh, J. Appl. Phys. **109**, 103913 (2011).
[31] O. Mosendz, J. E. Pearson, F. Y. Fradin, G. E. W. Bauer, S. D. Bader, and A. Hoffmann, Phys. Rev. Lett. **104**, 046601 (2010).
[32] O. Mosendz, V. Vlaminck, J. E. Pearson, F. Y. Fradin, G. E. W. Bauer, S. D. Bader, and A. Hoffmann, Phys. Rev. B **82**, 214403 (2010).
[33] K. Ando, Y. Kajiwara, S. Takahashi, S. Maekawa, K. Takemoto, M. Takatsu, and E. Saitoh, Phys. Rev. B **78**, 014413 (2008).
[34] H. Y. Inoue, K. Harii, K. Ando, K. Sasage, and E. Saitoh, J. Appl. Phys. **102**, 083915 (2007).
[35] K. Ando, T. Yoshino, and E. Saitoh, Appl. Phys. Lett. **94**, 152509 (2009).
[36] K. Ando, J. Ieda, K. Sasage, S. Takahashi, S. Maekawa, and E. Saitoh, Appl. Phys. Lett. **94**, 262505 (2009).
[37] T. Yoshino, K. Ando, K. Harii, H. Nakayama, Y. Kajiwara, and E. Saitoh, Appl. Phys. Lett. **98**, 132503 (2011).
[38] K. Harii, T. An, Y. Kajiwara, K. Ando, H. Nakayama, T. Yoshino, and E. Saitoh, J. Appl. Phys. **109**, 116105 (2011).
[39] Y. Kajiwara, K. Harii, S. Takahashi, J. Ohe, K. Uchida, M. Mizuguchi, H. Umezawa, H. Kawai, K. Ando, K. Takanashi, S. Maekawa, and E. Saitoh, Nature (London) **464**, 262 (2010).
[40] C. W. Sandweg, Y. Kajiwara, K. Ando, E. Saitoh, and B. Hillebrands, Appl. Phys. Lett. **97**, 252504 (2010).

[41]K. Ando, S. Takahashi, J. Ieda, H. Kurebayashi, T. Trypiniotis, C. H. W. Barnes, S. Maekawa, and E. Saitoh, Nat. Mater. **10**, 655 (2011).

[42]A. Azevedo, L. H. Vilela-Leao, R. L. Rodriguez-Suarez, A. F. Lacerda Santos, and S. M. Rezende, Phys. Rev. B **83**, 144402 (2011).

[43]F. D. Czeschka, L. Dreher, M. S. Brandt, M. Weiler, M. Althammer, I.-M. Imort, G. Reiss, A. Thomas, W. Schoch, W. Limmer, H. Huebl, R. Gross, and S. T. B. Goennenwein, Phys. Rev. Lett. **107**, 046601 (2011).

[44]K. Ando, T. An, and E. Saitoh, Appl. Phys. Lett. **99**, 092510 (2011).

[45]C. Kittel, *Introduction to Solid State Physics*, 8th ed. (Wiley, New York, 2005).

[46]H. Kurt, R. Loloee, K. Eid, W. P. Pratt, Jr., and J. Bass, Appl. Phys. Lett. **81**, 4787 (2002).

[47]The relation between $g_{\mathrm{eff}}^{\uparrow\downarrow}$ and $g^{\uparrow\downarrow}$ is described as $(g_{\mathrm{eff}}^{\uparrow\downarrow})^{-1} = (g^{\uparrow\downarrow})^{-1} + \beta$ (see Eq. 74 in Ref. 13), where β is the backflow factor expressed by $\beta = 1/(2\sqrt{\varepsilon/3}g^{\uparrow\downarrow}\tanh(d_N/\lambda))$ originating from the spin accumulation at the interface. While $g^{\uparrow\downarrow}$ represents intrinsic interface mixing conductance, which is independent of β, $g_{\mathrm{eff}}^{\uparrow\downarrow -1}$ includes the effect of the spin accumulation at the interface as an additional term β. As is clear in the equation, β never reduces to zero even at infinity of d_N, leaving the effect of the element-dependent factor ε.

[48]A. A. Abrikosov and L. P. Gor'kov, Zh. Eksp. Teor. Fiz. **42**, 1088 (1962) [Sov. Phys. JETP **15**, 752 (1962)].